Special-purpose elements to impose Periodic Boundary Conditions for multiscale computational homogenization of composite materials with the explicit Finite Element Method

S. Sádaba[1], M. Herráez[1,2], F. Naya[1,2], C. González[1,2], J. Llorca[1,2], C.S. Lopes[1*]

[1] *IMDEA Materials Institute, C/Eric Kandel 2, 28906 - Getafe, Madrid, Spain*

[2] *Dpto. Ciencia de Materiales, Universidad Politécnica de Madrid, E.T.S. de Ingenieros de Caminos, 28040 Madrid, Spain*

Abstract

A novel methodology is presented to introduce Periodic Boundary Conditions (PBC) on periodic Representative Volume Elements (RVE) in Finite Element (FE) solvers based on dynamic explicit time integration. This implementation aims at overcoming the difficulties of the explicit FE method in dealing with standard PBC. The proposed approach is based on the implementation of a user-defined element, named a Periodic Boundary Condition Element (PBCE), that enforces the periodicity between periodic nodes through a spring-mass-dashpot system. The methodology is demonstrated in the multiscale simulation of composite materials. Two showcases are presented: one at the scale of computational micromechanics, and another one at the level of computational mesomechanics. The first case demonstrates that the proposed PBCE allows the homogenization of composite ply properties through the explicit FE method with increased efficiency and similar reliability with respect to the equivalent implicit simulations with traditional PBC. The second case demonstrates that the PBCE coupled with Periodic Laminate Elements (PLE) can effectively be applied to the computational homogenization of elastic and strength properties of entire laminates taking into account highly nonlinear effects. Both cases motivate the application of

*Corresponding author: claudiosaul.lopes@imdea.org

the methodology in multiscale virtual testing in support of the building-block certification of composite materials.

Keywords: Explicit FEM, Periodic Boundary Conditions (PBC), Homogenization, Multiscale computational mechanics, Composite materials

1. Introduction

With the advances in computing power and the growing costs associated to physical experiments for certification of composites, multiscale virtual testing based on the Finite Element Method (FEM) has become a popular approach in the characterization and evaluation of composite materials and structures [1]. This approach often requires homogenization techniques, as the physical response of composite materials at the macroscale is a direct consequence of their microstructural features and architecture. Moreover, the behaviour of the composite might depend on microstructural features other than the properties and topology of the microconstituents (fibres, matrix and interfaces), such as fibre volume fraction, fibre size and shape distributions, distance between neighbouring fibres, voids, among others. Computational homogenization techniques are ideal tools to take all these effects into account.

The elastic, plastic and fracture responses of laminated Fibre Reinforced Polymers (FRP) at the macroscale can be computed efficiently by following a stepwise bottom-up multiscale approach [1–3]. In the first step, *computational micromechanics* is employed to predict the homogenized behaviour of a unidirectional fibre-reinforced yarn or ply, in 2D (e.g. [4–7]) or 3D spaces (e.g. [8–11]), with input properties resulting from the experimental characterization of the composite microconstituents: fibre [12], matrix [7] and fibre/matrix interface [13]. In the case of ply architectures with higher complexity than unidirectional fibres, such as in textile composites, a subsequent homogenization step needs to be performed based on the previously computed behaviour of the unidirectional yarns, the response of the bulk resin matrix and on the topology of the Representative Unit Cell (RUC) of the fabric (e.g. [14–17]). From the orthotropic ply behaviour and lamina orientations within a ply stacking, *computational mesomechanics* can be used to predict the behaviour of the laminate (e.g. [18–20]). At this step the response of the discrete ply interfaces also needs to be taken into account because laminated FRP are prone to delamination. The homogenized behaviour of the laminate can then be applied to the design of composite laminated structures by employing *computational structural mechanics* [1–3]. Some of these modelling techniques impose severe non-linearities to the respective numerical problems which become intractable by implicit integration FE solvers due to convergence difficulties. In such cases, explicit numerical schemes become the only viable alternative to achieve meaningful numerical predictions.

In the framework of multiscale modelling, the use of Representative Volume Elements (RVE) has become a very popular numerical approach for the purpose of homogenization in highly heterogeneous materials. This technique allows the reproduction of uniform stress states in a domain and thus, the prediction of homogenized thermo-mechanical properties as elasticity and strength. Apart from the selection of the RVE size, which must be sufficient to capture the stress-strain response and failure mechanisms of the composite, the applied boundary conditions play a key role on the assessment of the homogenized properties. There are three common types of boundary conditions: uniform boundary displacements or isostrain (Hill-Reuss), uniform boundary tractions or isostress (Hill-Voigt) and Periodic Boundary Conditions (PBC). The use of PBC on the RVE boundaries implies that smaller analysis domains are sufficient to obtain reliable homogenized properties [21]. Due to this reason, PBCs have been extensively employed in computational homogenization.

The classical approach to introduce PBC in a RVE is by means of the definition of strong relations (equations) between periodic nodes, hence imposing constraints to their allowed displacements. In its essence, this method requires the mesh to be periodic, in such a way that every node on each RVE boundary has its homologous node on the respective opposite (periodic) boundary, although enhancements, based on polynomial interpolation [22, 23] and Lagrange multipliers [24], have been proposed in order to avoid the need of matching the mesh topology on opposite RVE boundaries. Either way, the traditional PBC approach is well appropriate for implicit integration numerical schemes but the fulfilment of the periodicity equations in dynamic explicit time integration solvers tends to lead to spurious displacement oscillations that compromise the numerical solution. To overcome this issue, this work proposes the imposition of PBC in explicit FE solvers through special-purpose elements, named *Periodic Boundary Condition Elements* (PBCE). The paper demonstrates that this approach is specially well suited for multiscale computational analyses of composite materials and constitutes an enabling technology for multiscale computational homogenization in composite materials.

The formulation of the PBCE for general 3D FE problems and its implementation as a user-defined element in Abaqus/Explicit [25] are detailed in section 2. The reliability, applicability and efficiency of the approach are then demonstrated in the framework of multiscale computational analysis of composites, in section 3. First, the PBCE method in combination with RVE is applied to micromechanical homogenization of unidirectional FRP yarns or plies. The results are evaluated through the correlation of numerical results obtained with traditional PBC and new PBCE. Then, PBCE in combination with Representative Laminate Elements (RLE) are proposed for the homogenization of laminate behaviour through computational mesomechanics. Finally, the concluding remarks are drawn in section 4.

2. Periodic Boundary Condition Element

2.1. Definition

Periodic Boundary Conditions (PBC) guarantee the periodicity of the mechanical fields and ensure the continuity between neighbouring Representative Volume Elements (RVE), as in a jigsaw puzzle. The PBC are set by enforcing that the difference between displacement vectors, $\mathbf{u}$, of opposite sides of an RVE of lengths $\ell_1 \times \ell_2 \times \ell_3$ is equal to a relative displacement, $\mathbf{U}_i$. In mathematical form:

$$\begin{aligned}
\boldsymbol{\varphi}_1(x_2, x_3, \mathbf{U}_1) = (\mathbf{u}(0, x_2, x_3) - \mathbf{u}(\ell_1, x_2, x_3)) - \mathbf{U}_1 = \mathbf{0} \\
\boldsymbol{\varphi}_2(x_1, x_3, \mathbf{U}_2) = (\mathbf{u}(x_1, 0, x_3) - \mathbf{u}(x_1, \ell_2, x_3)) - \mathbf{U}_2 = \mathbf{0} \\
\boldsymbol{\varphi}_3(x_1, x_2, \mathbf{U}_3) = (\mathbf{u}(x_1, x_2, 0) - \mathbf{u}(x_1, x_2, \ell_3)) - \mathbf{U}_3 = \mathbf{0}
\end{aligned} \tag{1}$$

wherein $\boldsymbol{\varphi}_{i=1,3}$ are the three constraint equations relating relative displacements $\mathbf{U}_{i=1,3}$ of pairs of opposite nodes in the RVE sides, and $x_{i=1,3}$ are degrees of freedom (DOFs) in three dimensional space. The constraints can be introduced in the discrete potential energy associated to the weak form of the elastic equilibrium problem:

$$\Pi^h(\mathbf{u}^h) = \frac{1}{2}\int_{\Omega^h} \boldsymbol{\sigma}(\mathbf{u}^h) \cdot \nabla \mathbf{u}^h \, d\Omega - \int_{\Omega^h} \mathbf{u}^h \cdot \mathbf{f} \; d\Omega - \int_{\partial\Omega^h} \mathbf{u}^h \cdot \mathbf{h} \; d(\partial\Omega) + \sum_{i=1}^{3} \Psi_i(\mathbf{u}^h) \tag{2}$$

wherein $\boldsymbol{\sigma}(\mathbf{u}^h)$ and $\nabla\mathbf{u}^h$ stand for the stress and strain tensors associated to the discrete displacement field $\mathbf{u}^h$, and $\mathbf{f}$ and $\mathbf{h}$ are the body forces and contact stresses at the volume and boundary of the solid, respectively. Finally, $\Psi_i(\mathbf{u}^h)$ represents the potential energy associated to the introduction of the periodicity constraints. In the case of explicit time integration, equation 2 can be generalized to the dynamic problem by introducing the inertia and damping forces in the system.

The constraint equations (1) can be rearranged to obtain a more appropriate form for the FEM assembly procedure. For the easy imposition of PBC, the *global* reference nodes (master nodes) M_i and M'_i are defined such that $\mathbf{U}_i = \mathbf{u}_{M_i} - \mathbf{u}_{M'_i}$, as represented in Figure 1a.

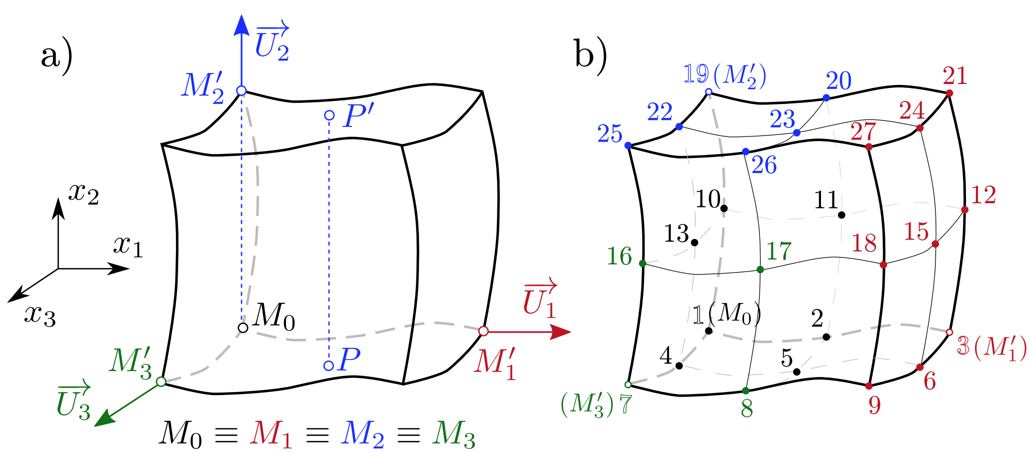

Figure 1: a) Four nodes involved in the PBC of displacement of nodes $P - P'$: M_2, M'_2, P, P'. b) Example FE model with $3 \times 3 \times 3$ nodes illustrating the coupling between periodic nodes.

The relative motion between a *local* point P belonging to a given plane of the RVE and point P' on the parallel plane displaced ℓ_i (length of the RVE in the direction i) can be expressed as a 4-point condition (Figure 1a),

$$\boldsymbol{\varphi}_i(\mathbf{u}_P, \mathbf{u}_{P'}, \mathbf{u}_{M_i}, \mathbf{u}_{M'_i}) = (\mathbf{u}_P - \mathbf{u}_{P'}) - \mathbf{U}_i = (\mathbf{u}_P - \mathbf{u}_{P'}) - (\mathbf{u}_{M_i} - \mathbf{u}_{M'_i}) = \mathbf{0} \quad (3)$$

for *all* pair of opposite nodes P and P', being $\overline{OP'} = \overline{OP} + \ell_i\mathbf{e}_i$ wherein $\mathbf{e}_i$ is the unit vector perpendicular to the RVE planes. In this regard, $\mathbf{u}_{M_i}$ and $\mathbf{u}_{M'_i}$ are selected to reproduce periodic homogeneous strain states through

Table 1: Boundary conditions applied through the master nodes (M'_1, M'_2, M'_3), where '0' represents a fixed DOF, '$-$' is a free DOF and δ a prescribed displacement.

Load case	$\mathbf{u}_{M'_1} = \overrightarrow{U_1}$	$\mathbf{u}_{M'_2} = \overrightarrow{U_2}$	$\mathbf{u}_{M'_3} = \overrightarrow{U_3}$
Uniaxial (1-direction)	$(\delta, 0, 0)$	$(0, -, 0)$	$(0, 0, -)$
Uniaxial (2-direction)	$(-, 0, 0)$	$(0, \delta, 0)$	$(0, 0, -)$
Pure shear (12-direction)	$(-, \delta, 0)$	$(0, -, 0)$	$(0, 0, -)$

the model. For simplicity, the displacement of the reference nodes, M_i, is set to zero to prevent rigid body motion of the whole model whereas the displacement of the master nodes, M'_i, depends on the loading case selected (see Table 1). Combined loading can be applied by superposition of boundary conditions for uniaxial and pure shear loading cases.

Due to compatibility reasons, periodic boundary conditions cannot be applied to every pair of periodic nodes. This is the case for node pairs (P, P') that belong to more than one PBC (edges and vertices). As a general rule, a P' node can only be part of one PBC. This is illustrated in Figure 1b for an example model with $3 \times 3 \times 3$ nodes in which each group of P' nodes is shown in a different color (red, blue and green), each color corresponding to the coupling with a reference master node (M'_1, M'_2, M'_3, respectively).

The linear constraint [26] between the displacements of these four points in equation 3 can be defined as:

$$\boldsymbol{\varphi}^e(\mathbf{u}_P, \mathbf{u}_{P'}, \mathbf{u}_M, \mathbf{u}_{M'}) = \mathbf{L}\mathbf{u}^e =$$

$$= \begin{bmatrix} 1 & 0 & 0 & -1 & 0 & 0 & -1 & 0 & 0 & 1 & 0 & 0 \\ 0 & 1 & 0 & 0 & -1 & 0 & 0 & -1 & 0 & 0 & 1 & 0 \\ 0 & 0 & 1 & 0 & 0 & -1 & 0 & 0 & -1 & 0 & 0 & 1 \end{bmatrix} \begin{bmatrix} u_P^1 \\ u_P^2 \\ u_P^3 \\ u_{P'}^1 \\ u_{P'}^2 \\ u_{P'}^3 \\ u_M^1 \\ u_M^2 \\ u_M^3 \\ u_{M'}^1 \\ u_{M'}^2 \\ u_{M'}^3 \end{bmatrix} = \mathbf{0} \qquad (4)$$

where u_P^i corresponds to the i-component of the displacement vector of node P.

Instead of satisfying the constraint exactly, a penalty approach is used such that the deviation from the exact fulfilment of the constraint penalizes the potential energy. The value selected for the penalty stiffness, k, should be high enough to make periodicity as accurate as possible. If the constraint $\boldsymbol{\varphi}^e = \mathbf{0}$ is verified, the element-wise elastic potential is minimum,

$$\Psi^e(\mathbf{u}^e) = \frac{1}{2}k\, \boldsymbol{\varphi}^e(\mathbf{u}^e) \cdot \boldsymbol{\varphi}^e(\mathbf{u}^e) = \frac{1}{2}k\, \mathbf{L}\mathbf{u}^e \cdot \mathbf{L}\mathbf{u}^e \tag{5}$$

and the internal forces necessary to obtain a good approximation of the constraints are calculated from the gradient of the potential, according to:

$$\left(\frac{\partial \Psi^e}{\partial \mathbf{u}^e}\right) = k\, \mathbf{L}^T\mathbf{L}\mathbf{u}^e = \mathbf{F}_k^e \tag{6}$$

This approach can be seen as a generalized spring network between nodes belonging to the boundaries, pulling the system back to the periodic constraint. Hence, its natural implementation in an explicit time integration FE solver such as Abaqus/Explicit [25] is by means of 4-node user-defined non-volumetric elements, henceforth named Periodic Boundary Condition Elements (PBCE), defined by means of a subroutine `VUEL`. The application of these user element implies the replacement of each set of PBC constraint equations (1) by a PBCE. Each PBCE enforces a local "penalty" constraint between opposite nodes P, P', and master nodes M_i, M_i' (Figure 1a) similar to the classic PBC (equations 1). The points $\{M_i, M_i'\}$ are assembled to be the same for each pair of opposite surfaces so that the globally-imposed displacement difference $\mathbf{U}_i$, is the same for all pairs of opposite nodes P, P'.

The *global* constraint $\Psi_i(\mathbf{u}^h)$ and the external forces $\mathbf{F}_{ext}$ appear naturally when the elements associated with the nodes belonging to the domain boundaries are assembled, and the displacements/forces are imposed to the master nodes. The constraint is satisfied approximately for each pair of opposite nodes. With the PBCE, the displacements of nodes M_i are constrained, whereas the displacements of nodes M_i' are imposed (Figure 1a).

It should be noted that either relative displacements $\mathbf{U}_i$ or forces $\mathbf{F}_i$ can be externally imposed through the master nodes. For instance, recalling Table 1, a uniaxial test in the direction 3 is imposed by means of $\mathbf{U}_3 = (0, 0, \bar{\epsilon}_3\ell_3)$ and $\mathbf{U}_1 = (u_1, 0, 0)$ and $\mathbf{U}_2 = (0, u_2, 0)$, being $\bar{\epsilon}_3$ the average strain imposed to the RVE along direction 3. In this case, u_1 and u_2 stand for the output lateral Poisson contraction resulting from the FEM computation.

As it is presented, this method originates undamped oscillations in dynamic analyses, as verified in preliminary simulations. Hence, damping mechanisms are implemented in the PBCE while preventing that its valid motions are affected. Viscous Rayleigh damping gives a force proportional to the negative rate of change of $\mathbf{L}\dot{\mathbf{u}}^e$ and parallel to the elastic force:

$$\mathbf{F}_c^e = c\, \mathbf{L}^T \mathbf{L} \dot{\mathbf{u}}^e \tag{7}$$

where c is a damping coefficient. For low loading rates, for which the effect of inertial forces is negligible, an additional mass m can be added to the system in the same way:

$$\mathbf{F}_m^e = m\, \mathbf{L}^T \mathbf{L} \ddot{\mathbf{u}}^e \tag{8}$$

Finally, the resulting equation of motion of the element, taking into account the external forces, becomes

$$\mathbf{0} = \mathbf{F}_k^e + \mathbf{F}_c^e + \mathbf{F}_m^e - \mathbf{F}_{ext}^e = \mathbf{L}^T \mathbf{L}(k\mathbf{u}^e + c\dot{\mathbf{u}}^e + m\ddot{\mathbf{u}}^e) - \mathbf{F}_{ext}^e \tag{9}$$

2.2. Stiffness, damping and mass parameters

The selection of the parameters k, c and m of the PBCE must be done according to a compromise between the accuracy of the results and the computational cost. For instance, high values of k would increase the accuracy of the periodic condition, nevertheless, the critical stable time increment of the PBCE ($\Delta t_{stab}^{\mathrm{PBCE}}$) would be reduced, increasing the number of increments to complete the simulation.

Based on equation 9, the Courant-Friedrichs-Lewy (CFL) condition [27] can be analysed for the derived PBCE to obtain the stable time increment of the user element as,

$$\Delta t_{stab}^{\mathrm{PBCE}} \approx \frac{2}{\omega} \cdot \left(\sqrt{1+\xi^2} - \xi \right) \tag{10}$$

where the angular frequency of the user element is $\omega = 2\sqrt{k/m}$, and $\xi = c/\sqrt{km}$.

Two examples on how to select these parameters are described in Sections 3.1 and 3.2.

3. Multiscale computational applications

The traditional approach to implement PBC is by means of constraint equations (`*EQUATION` in Abaqus [25]). This method has strong foundations for implicit solvers based on static equilibrium, but exhibits several drawbacks when explicit dynamic time integration (i.e. central differences) is used. It is observed that the relationships between master and slave displacements is translated into equations that introduce intense high-frequency oscillations in the system. It has not been possible to identify the exact cause for this behaviour which is possibly related to implementation difficulties in explicit algorithms. Related difficulties might be in the origin of the limitation in the number of supported constraint equations [1]. Moreover, the method with traditional PBC is computationally expensive. The Periodic Boundary Condition Element (PBCE) approach proposed in this paper is more efficient under similar conditions and it is not limited in the number of periodic DOF's.

In the following, the PBCE method is applied and validated under two computational homogenization scenarios in composite materials: micromechanical and mesomechanical homogenization.

3.1. Micromechanical homogenization

Micromechanical homogenization in composite materials is generally used to compute the elastic and strength properties of an orthotropic lamina and predict ply failure envelopes, e.g. [5–7, 11]. The behaviour of the ply transverse to the fibres direction can be analysed with two-dimensional or quasi-2D RVE, as shown in Figure 2. Herewith, a 2D version of the PBCE presented above is used in the computation of transverse tensile properties of the unidirectional Carbon-Fibre Reinforced Polymer (CFRP) material AS4/8552.

The microstructure of the RVE of an unidirectional composite is idealized as a dispersion of parallel and circular fibres randomly distributed in the polymer matrix. A minimum of 50 fibres is generally enough to capture adequately the essential features of the microstructure of the material while maintaining reasonable computing efforts, as demonstrated by González and LLorca [28]. Synthetic fibre distributions statistically equivalent to the real

[1] In Abaqus, this limit has been increased from version to version, being around 90000 for v6.14 [25]

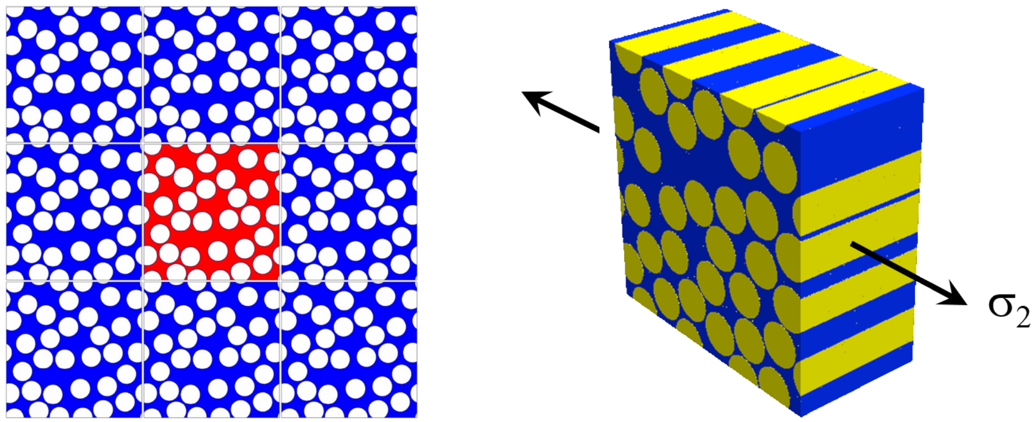

Figure 2: The composite mechanical behaviour is determined by solving numerically the boundary value problem for a RVE of the composite which is much larger than the heterogeneities in the microstructure.

ones are generated with a modified Random Sequential Adsorption (RSA) algorithm [8].

The RVE is discretized in Abaqus/Explicit [25] in the following way: the matrix and the fibres are modelled with 4-node fully integrated quadrilateral isoparametric elements under the assumption of plane strain (CPE4), while the fibre-matrix interface debonding is simulated with 4-node cohesive isoparametric elements (COH2D4) inserted at the interfaces between fibres and matrix. Perfect and homogeneous contact between fibres and matrix is assumed. The carbon fibres are assumed to behave as linear elastic transversely isotropic solids. The matrix is modelled as an isotropic elastic-plastic solid according to a modified Drucker-Prager plasticity yield surface including damage [25, 29]. The fibre-matrix interface behaviour follows a mixed-mode bilinear traction-separation law [25]. Detailed information about the constitutive models and material properties can be found in [4, 7].

A reference analysis was carried out with Abaqus/Standard [25] within the framework of the finite deformations theory. In addition, explicit dynamic analyses employing the default Abaqus/Explicit [25] PBC scheme, by means of constraint equations, were also run for comparison with the developed PBCE approach. In each analysis, an initial thermo-mechanical loading step simulates the cooling-down process from curing to service temperatures, given the significant influence of the respective residual stresses on the homogenized properties. This stage is followed by the application of mechanical load up to failure. Two typical load-cases were analysed herein: uniaxial transverse tension and transverse compression.

A careful selection of the mechanical parameters of the PBCE was done in advance to maximize the accuracy of the simulation without penalizing its computational cost. To this end, m was selected as the average nodal mass of the model ($m = 3.73 \cdot 10^{-7}$ g) such that no remarkable mass concentration would take place along the boundaries. In order for the PBCE to provide a good approximation of the periodicity condition, k must be high compared to the overall stiffness of the model (on each direction),

$$k \cdot N_e \gg k_{\text{model}} \tag{11}$$

where the stiffness of the model in the transverse direction is $k_{\text{model}} = E_2 \cdot A/L \approx 10^4$ N/m, and N_e is the number of user elements in the transverse direction ($N_e \approx 100$). A value of $k = 10^5$ N/m was found to be enough for the current analyses. Based on preliminary simulations, a value of $c = 0.001$ N s/m for the damping coefficient was sufficient to remove spurious oscillations. This combination of parameters did not penalize the stable time increment of the simulation, i.e. $\Delta t_{stab} < \Delta t_{stab}^{\text{PBCE}}$ (see equation 10).

Load was applied by means of a velocity-controlled profile following a smooth step to minimize shock waves that would introduce high inertial effects. For both load cases, the steady-state loading rate selected was $5 \cdot 10^{-4}$ m/s with a peak acceleration of 0.6 m/s^2.

The stress-strain curves resulting of the different analyses, as well as stress fields for the tensile cases and strain fields for the compression cases, are shown in Figure 3. For transverse tension, it is observed that the mechanical fields are equivalent between implicit and explicit analyses, and that ultimate failure is triggered by the same cracking mechanisms at similar applied stress level ($\approx$ 51.5 MPa) in both schemes. However, the explicit FE results using constraint equations (Explicit-PBC) are highly oscillatory and under-predict the transverse tensile strength of the material. For transverse compression, the match between implicit and explicit analyses with PBCE is again remarkable in terms of strain fields and load at failure ($\approx$ 205 MPa). The explicit analysis with constraint equations also shows an oscillatory response although the transverse compression strength obtained matches the one predicted by the two other schemes.

A summary of the computational cost associated to the solution of the

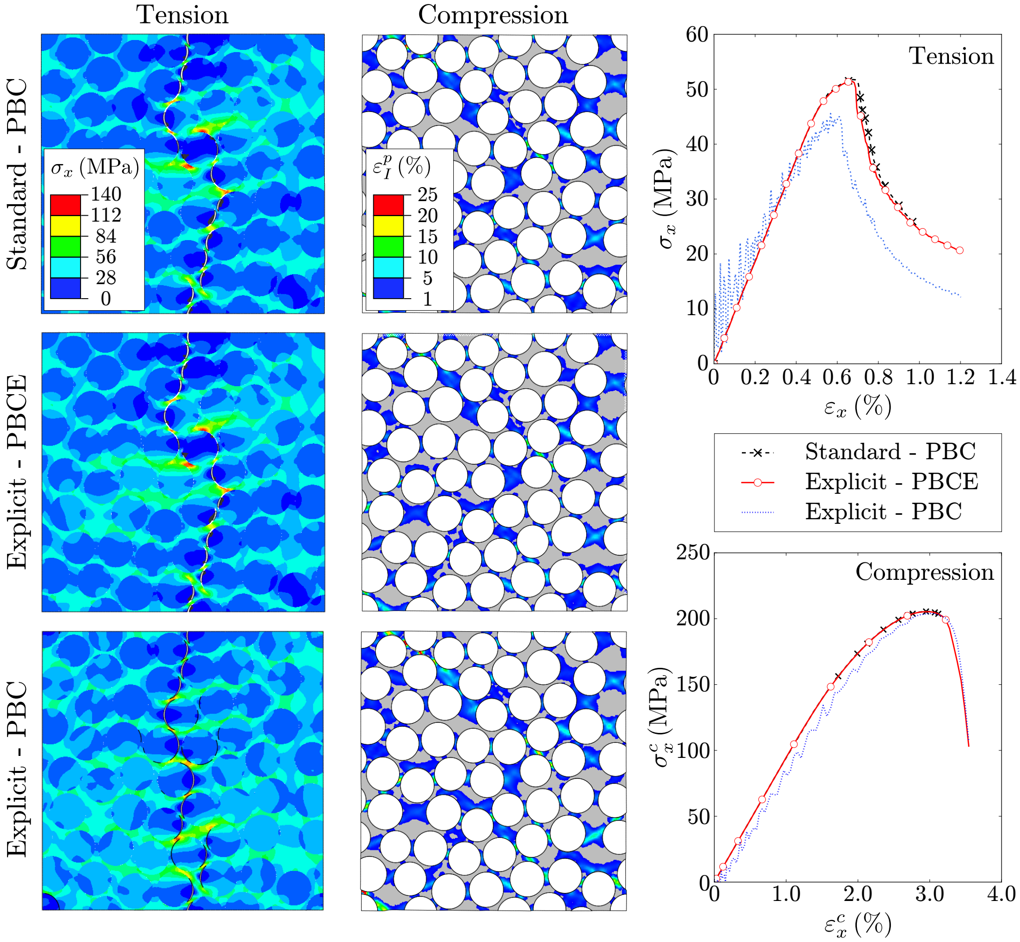

Figure 3: Comparison of the results obtained with Periodic Boundary Conditions Elements (PBCE) in Explicit against the Periodic Boundary Conditions (PBC) in Standard and Explicit by means of constraint equations. Transverse tension (left column) and compression (middle column) load cases are shown. The resulting stress-strain curves for each load case (tension and compression) for the three different schemes are shown in the right column.

tensile loading case by each of the numerical schemes is given in Table 2. For a fair comparison, all calculations were performed in a single CPU (Intel® Xeon® E5-2680 processor). In overview, the time required by the implicit solver (Abaqus/Standard) to complete the simulation is remarkably higher than for the explicit approaches. Nevertheless, the computation time required to reach the peak load point (value in parenthesis) is considerably lower for the implicit solver which takes advantage of the initial quasi-linearity of the problem by allowing large load increments at this stage. The explicit schemes are remarkably advantageous in the softening regime where the simulation becomes highly non-linear due the appearance of plastic deformation and damage. By comparing both explicit approaches, it is observed that the use of PBCE results in a $\approx 35\%$ reduction in computation time with respect to the traditional PBC scheme. The amount of memory required by the solver is also slightly reduced with the PBCE method ($\approx 10\%$).

Table 2: Comparison of the computational efficiency achieved with the PBCE scheme compared to the traditional solving schemes for the tensile load case (see Figure 3). In parenthesis, the computation time required to reach the peak load point.

Scheme	Computation time [s]	Memory required [Mb]
Standard - PBC	1766 (186)	32.0
Explicit - PBCE	800 (592)	16.9
Explicit - PBC	1055 (781)	19.3

3.2. Mesomechanical homogenization

The use of PBC at the mesoscale allows for the definition of a Representative Laminate Element (RLE), in essence a RVE of a laminate [18, 19], as represented in Figure 4. The use of PBC aims at introducing an uniform far-field stress to a small portion of the laminated material structure, assuming that the RLE behaviour is statistically representative of the whole specimen [30]. In this way, this approach allows the computation of the homogenized elastic and strength properties for a given laminate configuration in all orthotropic directions, and the prediction of a laminate failure envelope.

The traditional way to determine laminate properties and qualify composite materials for structural applications is done through costly and time consuming experimental testing following carefully devised test standards. In the recent years, numerical simulation arose as a promising alternative towards efficient material certification by virtual testing, with the added advantage that a much larger range of configurations can be considered [1, 2, 31]. The standard test methods can be modelled with high-fidelity and accurate predictions of laminate behaviour and relevant properties achieved, as demonstrated by Falcó et al. [20]. Both physical and virtual approaches aim

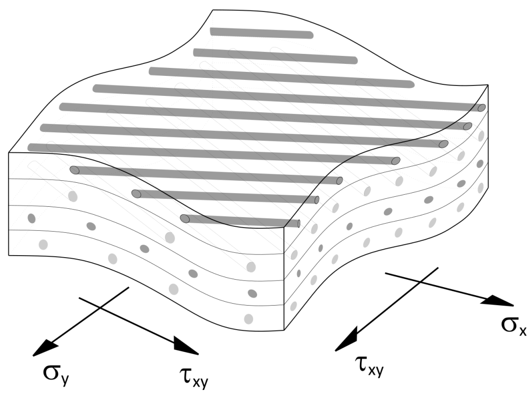

Figure 4: Representative Laminate Element (RLE).

at reproducing a macroscopically homogeneous stress state such that the resultant behaviour can be considered intrinsic to the laminate configuration. However, because of the finite width of the coupons and the three dimensional stress states at their edges [32, 33], the behaviour is significantly affected by edge cracking and delamination. By means of the RLE approach proposed in this paper, edge effects are removed from the boundaries of the numerical model and replaced by PBC, so that the analyses address only the material response. Moreover, the computational requirements are remarkably reduced since the RLE can be much smaller than the virtual coupon.

To capture the relevant mechanisms of laminate behaviour, the RLE domain is discretized in plies and ply interfaces. While interlaminar damage is assumed to occur in the form of delaminations along predefined and discrete crack planes, ply damage might occur in the form of fibre breakage, fibre pull-out, kink-banding and matrix cracking at any location within the plies. Hence, the appropriate description of the ply interface behaviour is achieved by means of cohesive and frictional relations between discrete fracture planes whilst the ply deformation mechanisms can be adequately tackled by means of a Continuum Damage Model (CDM) [20]. This modelling approach imposes severe instabilities, such as snap-back due to brittle cracking, to the numerical problem which typically result in convergence issues in implicit solvers. Therefore, the explicit numerical integration of the RLE, coupled with the PBCE proposed in this paper, constitutes the enabler of the computational homogenization of laminate behaviour.

For the purpose of demonstration, the In-Plane Shear (IPS) test on an AS4-8552 laminate is addressed herein. This experiment is used to characterize the in-plane shear response of a ±45 laminate, and is defined according to the ASTM D3518 test standard [34]. It consists of a rectangular coupon of $[\pm 45]_s$ configuration, 25 mm in width by up to 250 mm in length, loaded under quasi-static tension up to failure. To define an appropriate RLE, it is sufficient to consider an area of 10 x 10 mm^2 of the laminate to capture a representative number of intralaminar cracks for the element width employed (0.2 mm), as shown in Figure 5. Since the laminate at any point is statistically representative of the laminated structure, the only constraint on the dimensions of the RLE is that it should be much larger than the characteristic dimensions of the physical mechanisms that are to be simulated. In this case, the relevant phenomena are matrix cracking and delamination, which are associated to fracture process zones of the order of less than a millimetre [35]. Moreover, due to the out-of-plane symmetry of the $[\pm 45]_s$ configuration, only two plies (±45) need to be modelled with properly imposed symmetry boundary conditions.

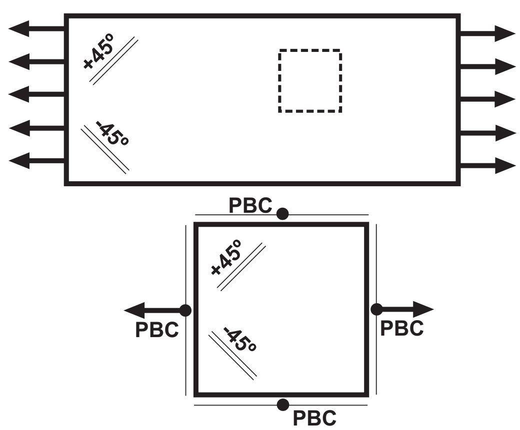

Figure 5: Illustrations of the In-Plane Shear (IPS) test (top) and the corresponding RLE (bottom) with applied PBCs and loads.

The laminate modelling approach follows the work of Falcó et al. [20]. Accordingly, the ply interface response is modelled by means of a general mixed-mode cohesive zone method coupled with frictional behaviour. The coupled cohesive-frictional approach is adopted to include the possible effects of ply friction during and after delamination, and is implemented in the kinematics of surface contact interaction algorithms available in Abaqus/Explicit [25]. The unidirectional FRP plies are modelled by means of a thermodynamicallyconsistent CDM that takes into account the relevant ply deformation mechanisms [20]. The nonlinear elastic-plastic shear behaviour of the material is modelled by a Ramberg-Osgood law [36]. The possibility of elastic unloading is tackled by means of a general elastic predictor - plastic corrector algorithm. The relevant ply and interface properties required by these models are given in [20]. Similar properties for the same material (different batches) are available in [37]. A regularized meshing approach is used, with material-alignment and directional biasing, as described in [20]. Each ply (0.184 mm in thickness) is discretized with a single through-the-thickness plane of regular 8-noded hexahedral isoparametric elements of 0.6 x 0.2 x 0.184 mm^3 in volume with reduced integration (C3D8R), except around the RLE edges wherein tetrahedral elements (C3D6R) are used.

As in the computational micromechanics case above, a judicious selection of the mechanical parameters of the PBCE was performed to ensure both the accuracy and the efficiency of the simulation. To this end, the PBCE damping and stiffness coefficients were set to $c = 0.1$ N s/mm and $k = 2 \cdot 10^5$ N/mm, respectively. The nodal mass of the PBCE was taken as the average nodal mass of the RLE.

Quasi-static tensile displacements were imposed to the RLE, as represented in Figure 5, until collapse was produced by the accumulation of matrix cracks and delamination between the +45^o and -45^o layers. For the purpose of qualitative correlation (Figure 6), the simulated accumulation of matrix cracks is compared with equivalent experimental results of an IPS test on a similar carbon/epoxy material which have been obtained by means of X-ray computed tomography (XCT) [38, 39].

In the experiments (Figure 6, left), cracks develop similarly in the +45^o and -45^o layers, starting from the edges of the specimen, following directions parallel to the fibres due to the kinematic constraints imposed by the microstructure. The crack density is always higher around the edges than in the specimen central sections and it increases with the applied load until saturation. Delamination also grows from the specimen edges. Finally, the accumulation of matrix cracking and delamination leads to instability and specimen collapse. The simulations on the smaller size RLE (Figure 6, right) capture this damage pattern while discarding the undesirable effects caused by the edges. It should be mentioned that, whilst the XCT is able to capture critical and sub-critical damage mechanisms, the simulations only predict the first, i.e. cracks completely developed through the thickness of the plies. Although the CDM does not contain information of the kinematic constraints

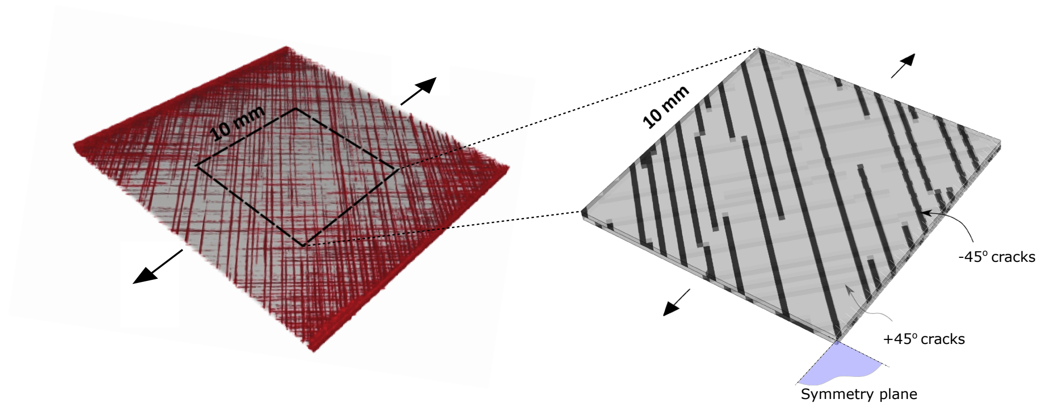

Figure 6: Qualitative correlation between experimentally-obtained (left) and simulated (right) development of matrix cracking in a plain stress $[\pm 45]_s$ laminate (experimental results adapted from [38]). Note: both experiments and simulations performed in similar carbon/epoxy $[\pm 45]_s$ coupons, although not exactly the same material.

imposed by the ply microstructure (the shear parallel and perpendicular to the fibre are represented with the same deformation tensor), this effect is obtained with the regularized meshing with material-alignment and directional biasing [20], leading to the correct simulation of crack directions. Hence, the RLE can be considered approximately representative of the central sections of the finite-width IPS coupon.

The results of the simulation in terms of the stress-strain behaviour are shown in Figure 7. The response of the RLE is nonlinear in a very similar way to the Ramberg-Osgood law [36] implemented at the constitutive level to describe the pure shear stress vs. shear strain relation of the ply, although not exactly since the IPS test configuration does not create pure shear on the ply but a mixed-mode loading situation, with a small fraction of transverse tension. For this same reason, the ultimate IPS load, IPSS = 99.7 MPa, also diverges from the ply shear strength, $S_L = 110.4$ MPa [37]. This demonstrates that this property is not adequately characterized by the IPS experiment [34], and a better alternative for that purpose is the Short Beam test standard ASTM D2344M [40] that measures the Interlaminar Shear Strength (ILSS) in a laminate.

Through-the-thickness matrix cracking, as shown in Figure 6, initiates at the highest load and deformation stages, rapidly growing and interacting with interface delamination to produce the collapse of the RLE. The simulated cracking is, however, not influenced by coupon edge effects as in the IPS

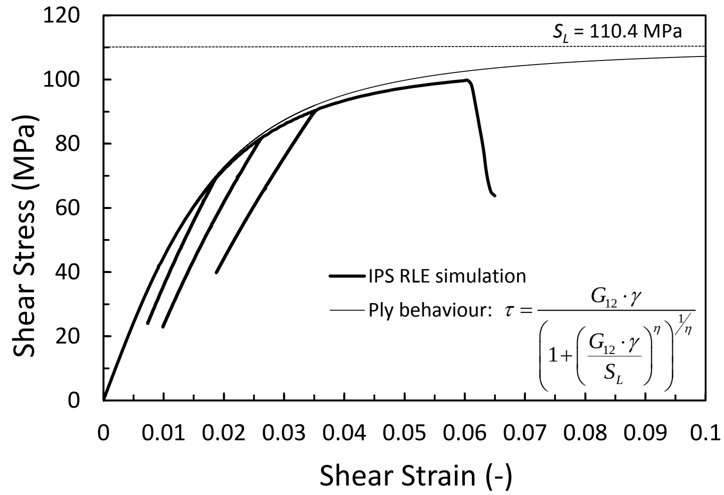

Figure 7: Stress-strain curves for the plain tension test. The appearance of the relevant damage events are marked with arrows in the figure. Ply in-plane shear strength, S_L = 110.4 MPa , measured by means of the Short Beam Test [37]. Numerically-obtained laminate In-Plane Shear Strength, IPSS = 99.7 MPa (at γ_{pl} = 0.04%). Experimentally-obtained $[\pm 45]_s$ specimen IPSS = 91.6 MPa (SD = 2.51 MPa) corresponding to $\gamma_{pl} = 0.05$ [37]. Ply in-plane shear modulus G_{12} = 4.9 GPa. Ramberg-Osgood exponential, $\eta = 1.9$.

experiment. As result, the numerically obtained In-Plane Shear Strength, IPSS = 99.7 MPa is higher than the average value obtained experimentally with the IPS experiment, IPSS = 91.56 MPa [37].

The numerically-obtained unloading-reloading behaviour of the RLE is also represented in Figure 7 to demonstrate that the PBCE, and the constitutive ply model, work well under these circumstances.

4. Conclusion

Special-purpose Periodic Boundary Condition Elements (PBCE) were proposed to impose Periodic Boundary Conditions (PBC) to general Representative Volume Elements (RVE) in FE solvers based on dynamic explicit time integration. This approach solves the issue of spurious oscillations resulting from the application of the traditional PBC approach in the explicit FEM, overcomes limitations in the number of constraint relations and allows gains in computational efficiency. The PBCE formulation was implemented by means of a user-defined element through a `VUEL` subroutine in Abaqus/Explicit [25]. The reliability and applicability of the approach were demonstrated in the framework of multiscale computational analysis of composites. First, the PBCE method in combination with RVE were applied to micromechanical homogenization of unidirectional FRP yarns or plies. The correlation between traditional PBC in implicit integration and PBCE in the explicit FEM was remarkable. Then, PBCE in combination with Representative Laminate Elements (RLE) were proposed and validated for the purpose of homogenization of laminate behaviour through computational mesomechanics to expedite the virtual testing of composite materials and eliminate undesired effects of coupon-based experiments.

Acknowledgements

The research leading to this publication was supported by the European Community FP7 Programme through project MAAXIMUS (grant agreement 213371) and by the Spanish Ministry of Industry, Economy and Competitiveness (MINECO) through project HYDTCOMP (grant MAT2015-69491-C03-02). C.S. Lopes also acknowledges the support of MINECO through the *Ramón y Cajal* fellowship (grant RYC-2013-14271). The authors are grateful to Prof. Ignacio Romero for his helpful insights on this research.

Data availability

The raw/processed data required to reproduce these findings cannot be shared at this time as the data also forms part of an ongoing study.

References

[1] C. S. Lopes, C. González, O. Falcó, F. Naya, J. Llorca, B. Tijs, Multiscale virtual testing: the roadmap to efficient design of composites for damage resistance and tolerance, CEAS Aeronautical Journal 7 (2016) 607–619.

[2] J. Llorca, C. González, J. M. Molina-Aldareguía, J. Segurado, R. Seltzer, F. Sket, M. Rodríguez, S. Sádaba, R. Muñoz, L. P. Canal, Multiscale modeling of composite materials: a roadmap towards virtual testing., Advanced materials 23 (2011) 5130–47.

[3] J. Llorca, C. González, J. Molina-Aldareguía, C. Lopes, Multiscale modeling of composites: Toward virtual testing... and beyond, The Journal of The Minerals, Metals & Materials Society (TMS) 65 (2013) 215–225.

[4] M. Herráez, C. González, C. Lopes, R. G. de Villoria, J. LLorca, T. Varela, J. Sánchez, Computational micromechanics evaluation of the effect of fibre shape on the transverse strength of unidirectional composites: An approach to virtual materials design, Composites Part A: Applied Science and Manufacturing 91 (2016) 484–492.

[5] A. Melro, P. Camanho, F. Andrade Pires, S. Pinho, Micromechanical analysis of polymer composites reinforced by unidirectional fibres: Part II Micromechanical analyses, International Journal of Solids and Structures 50 (2013) 1906–1915.

[6] T. Vaughan, C. McCarthy, A micromechanical study on the effect of intra-ply properties on transverse shear fracture in fibre reinforced composites, Composites Part A: Applied Science and Manufacturing 42 (2011) 1217–1228.

[7] F. Naya, C. González, C. S. Lopes, S. V. der Veen, F. Pons, Computational micromechanics of the transverse and shear behavior of unidirectional fiber reinforced polymers including environmental effects, Composites Part A: Applied Science and Manufacturing 92 (2017) 146–157.

[8] J. Segurado, J. Llorca, A numerical approximation to the elastic properties of sphere-reinforced composites, Journal of the Mechanics and Physics of Solids 50 (2002) 2107–2121.

[9] J. Williams, J. Segurado, J. LLorca, N. Chawla, Three dimensional (3D) microstructure-based modeling of interfacial decohesion in particle reinforced metal matrix composites, Materials Science and Engineering: A 557 (2012) 113–118.

[10] O. Pierard, C. González, J. Segurado, J. LLorca, I. Doghri, Micromechanics of elasto-plastic materials reinforced with ellipsoidal inclusions, International Journal of Solids and Structures 44 (2007) 6945–6962.

[11] F. Naya, M. Herráez, C. S. Lopes, C. González, S. V. der Veen, F. Pons, Computational micromechanics of fiber kinking in unidirectional FRP under different environmental conditions, Composites Science and Technology 144 (2017) 26 – 35.

[12] M. Herráez, A. Fernández, C. Lopes, C. González, Strength and toughness of structural fibres for composite material reinforcement, Philosophical Transactions of the Royal Society A 374 (2016) 1–11.

[13] F. Naya, J. M. Molina-Aldareguía, C. Lopes, C. González, J. Llorca, Interface characterization in fiber-reinforced polymer-matrix composites, The Journal of The Minerals, Metals & Materials Society (TMS) 69 (2017) 13–21.

[14] A. R. Melro, P. P. Camanho, F. M. Andrade Pires, S. T. Pinho, Numerical simulation of the non-linear deformation of 5-harness satin weaves, Computational Materials Science 61 (2012) 116–126.

[15] C. Zhang, W. K. Binienda, R. K. Goldberg, L. W. Kohlman, Meso-scale failure modeling of single layer triaxial braided composite using finite element method, Composites Part A: Applied Science and Manufacturing 58 (2014) 36–46.

[16] G. Anzelotti, G. Nicoletto, E. Riva, Mesomechanic strain analysis of twill-weave composite lamina under unidirectional in-plane tension, Composites Part A: Applied Science and Manufacturing 39 (2008) 1294–1301.

[17] A. García-Carpintero, M. Herráez, J. Xu, C. S. Lopes, C. González, A Multi Material Shell Model for the Mechanical Analysis of Triaxial Braided Composites, Applied Composite Materials 24 (2017) 1425–1445.

[18] Z. Xia, Y. Zhang, F. Ellyin, A unified periodical boundary conditions for representative volume elements of composites and applications, International Journal of Solids and Structures 40 (2003) 1907–1921.

[19] Y. Zhang, Z. Xia, F. Ellyin, Two-scale analysis of a filament-wound cylindrical structure and application of periodic boundary conditions, International Journal of Solids and Structures 45 (2008) 5322–5336.

[20] O. Falcó, R. L. Ávila, B. Tijs, C. S. Lopes, Modelling and simulation methodology for unidirectional composite laminates in a virtual test lab framework, Composite Structures 190 (2018) 137159.

[21] T. Kanit, S. Forest, I. Galliet, V. Mounoury, D. Jeulin, Determination of the size of the representative volume element for random composites:

Statistical and numerical approach, International Journal of Solids and Structures 40 (2003) 3647–3679.

[22] V. D. Nguyen, E. Béchet, C. Geuzaine, L. Noels, Imposing periodic boundary condition on arbitrary meshes by polynomial interpolation, Computational Materials Science 55 (2012) 390–406.

[23] J. M. Tyrus, M. Gosz, E. DeSantiago, A local finite element implementation for imposing periodic boundary conditions on composite micromechanical models, International Journal of Solids and Structures 44 (2007) 2972–2989.

[24] F. J. P. Reis, F. M. Andrade Pires, A mortar based approach for the enforcement of periodic boundary conditions on arbitrarily generated meshes, Computer Methods in Applied Mechanics and Engineering 274 (2014) 168–191.

[25] Abaqus version 6.14 online documentation, Analysis user's manual, Simulia Inc., Dassault Systèmes, 2013.

[26] R. E. Bridson, CPSC 426 computer animation, Department of Computer Science, University of British Columbia, $www.cs.ubc.ca/\sim rbridson/courses/533b-winter-2004/cs533b\_slides\_jan27.pdf$, 2004.

[27] R. Courant, K. Friedrichs, H. Lewy, Über die partiellen Differenzengleichungen der mathematischen Physik, Mathematische Annalen 100 (1928) 32–74.

[28] C. González, J. LLorca, Mechanical behavior of unidirectional fiber-reinforced polymers under transverse compression: Microscopic mechanisms and modeling, Composites Science and Technology 67 (2007) 2795–2806.

[29] D. C. Drucker, W. Prager, Soil mechanics and plastic analysis for limit design, Quarterly of Applied Mathematics 10 (1952) 157–165.

[30] J. Segurado, J. LLorca, A numerical approximation to the elastic properties of sphere-reinforced composites, Journal of the Mechanics and Physics of Solids 50 (2002) 2107 – 2121.

[31] J. LLorca, C. González, J. Molina-Aldareguía, C. Lópes, Multiscale modeling of composites: Toward virtual testing... and beyond, JOM 65 (2013) 215–225.

[32] R. B. Pipes, N. Pagano, Interlaminar stresses in composite laminates under uniform axial extension, Journal of Composite Materials 4 (1970) 538–548.

[33] C. Mittelstedt, W. Becker, The pipes–pagano-problem revisited: Elastic fields in boundary layers of plane laminated specimens under combined thermomechanical load, Composite Structures 80 (2007) 373 – 395.

[34] ASTM, Standard test method for in-plane shear response of polymer matrix composite materials by test of a $\pm 45^\circ$ laminate, Technical Report, American Society for Testing and Materials (ASTM), West Conshohocken, PA, USA, 1994. ASTM D3518/3518M-94.

[35] A. Turon, P. Camanho, J. Costa, C. Dávila, A damage model for the simulation of delamination in advanced composites under variable-mode loading, Mechanics of Materials 38 (2006) 1072–1089.

[36] W. Ramberg, W. R. Osgood, Description of stress-strain curves by three parameters, National Advisory Committee For Aeronautics (1943). Technical Note No. 902.

[37] NCAMP, Hexcel 8552 AS4 Unidirectional Prepeg Qualification Statical Analysis Report, Technical Report, National Center for Advanced Materials Performance, 2011. CAM-RP-2010-002 May 6, Revision A.

[38] F. Sket, A. Enfedaque, C. Alton, C. D. Gonzalez, J. M. Molina-Aldareguia, J. LLorca, Automatic quantification of matrix cracking and fiber rotation by x-ray computed tomography in shear-deformed carbon fiber-reinforced laminates., Composites Science and Technology 90 (2014) 129–138.

[39] F. Sket, M. Rodríguez-Hortalá, J. Molina-Aldareguía, J. Llorca, E. Maire, G. Requena, In situ tomographic investigation of damage development in $\pm$ 45° carbon fibre reinforced laminates, Materials Science and Technology 31 (2015) 587–593.

[40] ASTM, Standard Test Method for Short-Beam Strength of Polymer Matrix Composite Materials and Their Laminates, Technical Report, American Society for Testing and Materials (ASTM), West Conshohocken, PA, USA, 2000. ASTM D 2344-2344M(2000).